APS physics

CHORUS

This is the accepted manuscript made available via CHORUS. The article has been published as:

Electric-field-induced helium-helium resonances

Q. Guan and D. Blume

Phys. Rev. A **99**, 033416 — Published 19 March 2019

DOI: 10.1103/PhysRevA.99.033416

Electric-field induced helium-helium resonances

Q. Guan[1] and D. Blume[1]

[1]*Homer L. Dodge Department of Physics and Astronomy, The University of Oklahoma, 440 W. Brooks Street, Norman, Oklahoma 73019, USA*

(Dated: March 4, 2019)

The tunability of the helium-helium interaction through an external electric field is investigated. For a static external field, electric-field induced resonances and associated electric-field induced bound states are calculated for the ^{4}He-^{4}He, ^{3}He-^{4}He, and ^{3}He-^{3}He systems. Qualitative agreement is found with the literature for the ^{3}He-^{4}He and ^{3}He-^{3}He systems [E. Nielsen, D. V. Fedorov, and A. S. Jensen, Phys. Rev. Lett. **82**, 2844 (1999)]. The implications of the predicted electric-field induced resonances for ^{4}He-^{4}He on the wave packet dynamics, initiated by intense laser pulses, are investigated. Our results are expected to guide next generation experiments.

PACS numbers:

I. INTRODUCTION

The helium atom is a chemically inert rare gas atom. Helium has two naturally occuring isotopes: ^{4}He, a composite boson, and ^{3}He, a composite fermion. Whether or not these isotopes form diatomic molecules was debated for a long time in the literature. It is now agreed upon that the ^{4}He-^{4}He system supports a single rotationless bound state with an extremely small binding energy of about 1.3 mK [1–7]. Neither the ^{3}He-^{4}He nor the ^{3}He-^{3}He system support, in the absence of external fields, molecular bound states.

The extremely small binding energy of the ^{4}He-^{4}He dimer is associated with a large positive s-wave scattering length. The ^{3}He-^{4}He system, in contrast, is characterized by a negative and large, in magnitude, s-wave scattering length. Motivated by the tunability of many of the alkali dimers through the application of an external magnetic field in the vicinity of a Fano-Feshbach resonance [8], one may ask if the helium-helium interaction can be tuned as well, with the external magnetic field replaced by an external electric field. If such a tunability existed, this would open up many new research directions related to the study of extremely weakly-bound molecular states for a system that is amenable to *ab initio* calculations. Indeed, Ref. [9] pointed out the tunability of the ^{3}He-^{4}He and ^{3}He-^{3}He systems by a static external electric field. Moreover, Ref. [9] explored the consequences of this tunability for the three-body sector in the context of Efimov physics [10–12]. The tunability of the ^{4}He-^{4}He system by a static electric field and by laser pulses strong enough to involve electronically excited potential curves was very recently pointed out in Ref. [13].

Working in the opposite regime of short laser pulses, a recent molecular beam experiment [14] demonstrated that a short 310fs laser pulse with an intensity of a few times 10^{14}W/cm^2 can induce dissociative wave packet dynamics of the ^{4}He-^{4}He dimer, including interferences between the $l = 0$ and $l = 2$ partial wave channels. Here, l denotes the orbital angular momentum quantum number. While Ref. [14] provided no evidence for the existence of electric field-induced bound states or hybridized states such as those predicted in Ref. [15], the experimental results clearly show that the laser-molecule coupling is strong enough to trigger measurable changes such as a clean alignment signal. Moreover, the excellent agreement between the experimental and theoretical results in Ref. [14] suggests that the laser-molecule interaction, which included the lowest Born-Oppenheimer potential curve and assumed inertness of the electronic degrees of freedom, provides a reliable description, at least in the short-pulse regime for the intensities considered.

The present theoretical work considers laser pulses that are longer than those utilized in Ref. [14]. As a first exploration, our theoretical framework neglects, as in Ref. [14], the electronic degrees of freedom. It is expected that corrections due to the electronic motion (see, e.g., Ref. [16]) need to be accounted for in follow-up work. One of the goals is to explore under which conditions the electric-field induced resonances of the helium-helium systems, first investigated in Ref. [9] for the ^{3}He-^{4}He and ^{3}He-^{3}He systems and for the ^{4}He-^{4}He system in Ref. [13], can be observed experimentally in time-dependent set-ups. To interpret the dynamic wave packet studies, the static field case is revisited and some quantitative discrepancies with the literature [9], which we have no explanation for, are pointed out. To observe the electric-field induced resonances, the associated bound states have to be populated with sufficiently high probability and some signature that this has been achieved needs to be recorded. Our time-dependent calculations show, owing to the extremely floppy and highly quantum mechanical nature of the helium dimers, that revival dynamics competes with dissociative dynamics. Probing this intricate dynamics experimentally is expected to be possible but quite challenging due to the need of realizing long, intense laser pulses.

The remainder of this article is organized as follows. Section II introduces the system Hamiltonian and relevant theoretical background. Sections III and IV present our results for a static external field and a time-dependent external field, respectively. Last, Sec. V concludes.

II. SYSTEM HAMILTONIAN AND THEORETICAL BACKGROUND

This section describes the theoretical framework employed to investigate the tunability of the effective helium-helium interaction strength. Section II A introduces the system Hamiltonian. The determination of the scattering and bound states of the static Hamiltonian are discussed in Secs. II B and II C. Last, Sec. II D summarizes how the wave packet propagation is done when the Hamiltonian is time-dependent.

A. System Hamiltonian

We consider two helium atoms, either two ^{4}He atoms, a ^{3}He-^{4}He pair, or two ^{3}He atoms, with reduced mass μ interacting through the spherically-symmetric state-of-the-art "electronic ground state" potential $V_{2\mathrm{b}}(r)$ from Ref. [17], where $\vec{r}$ denotes the internuclear distance vector and r is equal to $|\vec{r}|$. Due to the adiabatic beyond Born-Oppenheimer correction term [17], the interaction potentials for ^{4}He-^{4}He, ^{3}He-^{4}He, and ^{3}He-^{3}He are slightly different.

Throughout we assume that the electric field of the laser is oriented along the z-axis. Moreover, we assume that the oscillations of the electric field are so fast that they can be integrated over. With these assumptions, the time-dependent laser-molecule interaction $V_{\mathrm{lm}}(r,\theta,t)$ reads [18]

$$V_{\mathrm{lm}}(r,\theta,t) = -\frac{1}{2}|\epsilon(t)|^2 \left[\alpha_{\parallel}(r)\cos^2\theta + \alpha_{\perp}(r)\sin^2\theta\right], \quad (1)$$

where θ denotes the angle between the z-axis and the internuclear distance vector $\vec{r}$ (in spherical coordinates, this is the azimuthal angle), $\epsilon(t)$ characterizes the shape of the laser pulse, and $\alpha_{\perp}(r)$ and $\alpha_{\parallel}(r)$ denote the polarizabilities perpendicular and parallel to the molecular axis. The difference between these polarizabilities is responsible for the intriguing dynamics discussed in Sec. IV.

Following the pioneering work of Buckingham and Watts [19], analytic expressions for $\alpha_{\perp}(r)$ and $\alpha_{\parallel}(r)$ read

$$\alpha_{\perp}(r) = 2\alpha_0 - \frac{2\alpha_0^2}{4\pi\mathcal{E}_0\, r^3} + \frac{2\alpha_0^3}{(4\pi\mathcal{E}_0)^2\, r^6} \quad (2)$$

and

$$\alpha_{\parallel}(r) = 2\alpha_0 + \frac{4\alpha_0^2}{4\pi\mathcal{E}_0\, r^3} + \frac{8\alpha_0^3}{(4\pi\mathcal{E}_0)^2\, r^6}, \quad (3)$$

where α_0 denotes the atomic polarizability, $\alpha_0 = 1.383 a.u.$ ("$a.u.$" stands for "atomic units"), and $\mathcal{E}_0$ the permittivity ($4\pi\mathcal{E}_0 = 1 a.u.$; note that the symbols ϵ and $\mathcal{E}_0$ refer to different physical quantities). To discuss the physics, we rewrite V_{lm} (in doing so, we drop the r-independent terms, which only contribute an energy shift and/or an overall phase),

$$V_{\mathrm{lm}}(r,\theta,t) = \frac{|\epsilon(t)|^2\alpha_0^2}{4\pi\mathcal{E}_0}\left[-\frac{2\alpha_0}{(4\pi\mathcal{E}_0)\, r^6} + \alpha_0\frac{1-3\cos^2\theta}{(4\pi\mathcal{E}_0)\, r^6} + \frac{1-3\cos^2\theta}{r^3}\right]. \quad (4)$$

The first term in square brackets shows that the laser-molecule interaction increases the C_6 van der Waals coefficient of the helium-helium potential. The second term in square brackets shows that the laser-molecule interaction introduces an angle-dependence into the C_6 coefficient. Finally, the third term in square brackets corresponds to the interaction between two point dipoles, yielding a repulsive interaction energy for a side-by-side configuration and an attractive interaction energy for a head-to-tail configuration. These analytic expressions agree well with the state-of-the-art *ab initio* results from Ref. [20] in the large r region but not in the small r region (see Fig. 1).

We find that the analytic expressions and the *ab initio* parametrization yield predictions that differ quantitatively but not qualitatively. The analytic polarizability model, for example, supports field-induced bound states for somewhat smaller field strengths than the *ab initio* parametrization. Similarly, the dynamical results presented in Sec. IV are dominated by the polarizabilities around $4 a.u.$ to $10 a.u.$ for which the two sets of polarizabilities agree quite well. Since the results for the two models agree qualitatively, the majority of the results presented in this work employs the polarization model from Ref. [20].

Since the Hamiltonian H is in our set-up independent of the polar angle ϕ, the projection quantum number m_l, which is associated with the z-component of the orbital angular momentum operator $\vec{l}$, is a good quantum number. We restrict ourselves to the $m_l = 0$ channel in this work. Combining the interaction terms, the time-dependent Hamiltonian H, written in spherical coordinates, reads

$$H = -\frac{\hbar^2}{2\mu}\left[\frac{1}{r^2}\frac{\partial}{\partial r}\left(r^2\frac{\partial}{\partial r}\right) + \frac{1}{r^2\sin\theta}\frac{\partial}{\partial\theta}\left(\sin\theta\frac{\partial}{\partial\theta}\right)\right] + V_{2\mathrm{b}}(r) + V_{\mathrm{lm}}(r,\theta,t). \quad (5)$$

We consider two parametrizations of $\epsilon(t)$:

1. Static field with $\epsilon(t) = \epsilon_{0,\mathrm{S}}$, where $\epsilon_{0,\mathrm{S}}$ is a constant. Even though some of the field strengths $\epsilon_{0,\mathrm{S}}$ considered in this work can only be realized for a relatively short time with present day technology, the results for the static field provide a useful framework for understanding the results for time-dependent pulses.

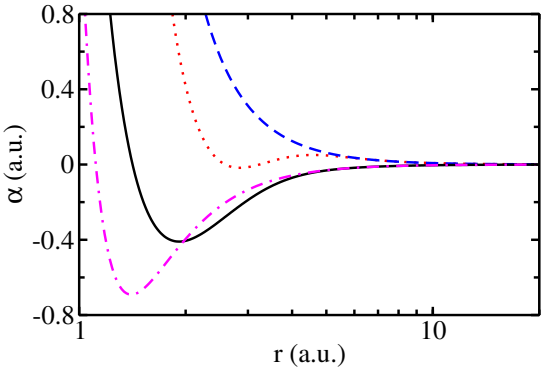

FIG. 1: (Color online) Polarizabilities as a function of the internuclear distance r (note the logarithmic scale of the horizontal axis). The solid and dotted lines show $\alpha_\perp$ and $\alpha_\parallel$ using the *ab initio* data from Ref. [20]. The dash-dotted and dashed lines show $\alpha_\perp$ and $\alpha_\parallel$ using the analytical polarizabilities [see Eqs. (2) and (3)]. The constant contribution of $2\alpha_0$ is not included in the plots.

2. A "stretched" Gaussian pulse with $\epsilon(t) = \epsilon_{\rm SG}(t)$,

$$\epsilon_{\rm SG}(t) = \begin{cases} \epsilon_{\rm G}(t) & \text{for } t \le 0 \\ \epsilon_{0,\rm G} & \text{for } 0 < t < t_{\rm hold} \\ \epsilon_{\rm G}(t - t_{\rm hold}) & \text{for } t_{\rm hold} \le t, \end{cases} \tag{6}$$

where

$$\epsilon_{\rm G}(t) = \epsilon_{0,\rm G} \exp\left(-2\ln(2)\frac{t^2}{\tau^2}\right) \tag{7}$$

with $\ln(2) = 0.6931\cdots$. At $t = 0$, the pulse is maximal for the first time and τ is the FWHM, which determines the rise and fall-off of the Gaussian pulse. While the stretched Gaussian pulse shape may not be realizable experimentally, the ensuing dynamics is comparatively straightforward to interpret and thus serves as a guide to what might be expected for stretched pulses with somewhat different profiles.

B. Scattering States

In the absence of the external field ($V_{\rm lm} = 0$), the s-wave scattering length a_s of the ^{4}He-^{4}He system is positive and large ($a_s = 170.9 a.u.$), signaling the existence of a weakly-bound molecular s-wave state. In fact, this is the only bound state supported in the field-free case; no rotationally or vibrationally excited states exist. The s-wave scattering length of the ^{3}He-^{4}He system, in contrast, is negative and large in magnitude ($a_s = -34.2 a.u.$), signaling that the system is just short of supporting a weakly-bound s-wave bound state. No deeply-lying bound states are supported. The s-wave scattering length of the ^{3}He-^{3}He system is equal to $-13.73 a.u.$ in the absence of an external electric field; in this case, the nuclear spins form a singlet, thereby enforcing the antisymmetry of the full wave function under the exchange of two identical ^{3}He atoms. The magnitude of the generalized higher partial wave scattering lengths such as the p-wave scattering volume for the ^{3}He-^{4}He and ^{3}He-^{3}He systems and the d-wave scattering hypervolume for the ^{4}He-^{4}He system are small.

We now include a time-independent laser-molecule Hamiltonian (parametrization 1. in Sec. II A), which couples different orbital angular momentum channels. For the bosonic ^{4}He-^{4}He system, only even-l channels contribute because the spatial wave function has to be symmetric under the exchange of the two ^{4}He atoms. For the ^{3}He-^{4}He system, in contrast, no symmetry constraints exist, implying that even- and odd-l channels contribute (due to the nature of the laser-molecule interaction, the even- and odd-l channels are decoupled). Last, for the fermionic ^{3}He-^{3}He system, even-l channels contribute when the nuclear spins form a singlet and odd-l channels when the nuclear spins form a triplet. The long-range nature of the laser-molecule interaction modifies the threshold law in the non-zero partial wave channels [21–24]. In particular, since the K-matrix elements $K_{l,l'}(k)$,

$$K_{l,l'}(k) = \tan\left(\delta_{l,l'}(k)\right), \tag{8}$$

are proportional to the wave vector k as k goes to zero (k is defined in terms of the scattering energy E through $\sqrt{2\mu E}/\hbar$), the zero-energy scattering length matrix elements $a_{l,l'}$ are defined through

$$a_{l,l'} = \lim_{k\to 0} \frac{-K_{l,l'}(k)}{k}. \tag{9}$$

For short-range interactions (interactions that fall off faster than $1/r^3$ at large internuclear distances), the denominator in Eq. (9) reads $k^{l+l'+1}$ instead of k [25]; the modification of the power of k reflects the modified threshold behavior. The threshold laws, Eqs. (8) and (9), depend crucially on the angle dependence of the $-r^{-3}$ potential. If the angle dependence was absent, one would not be able to define an s-wave scattering length.

The phase shifts $\delta_{l,l'}(k)$ [see Eq. (8)] are obtained by matching the inside solution to the large-r, free-particle solution, with the relative importance of the regular solutions [the spherical Bessel functions $j_l(kr)$] and the irregular solutions [the Neumann functions $n_l(kr)$] given by the tangent of the phase shifts $\delta_{l,l'}(k)$. The scattering solutions in the presence of a static external field are thus characterized by an, in general, non-diagonal scattering length matrix. Even though the determination of the scattering solutions requires the entire scattering length matrix, the emergence of a new zero-energy bound state

that is even (odd) in the relative coordinate z is accompanied by the $a_{0,0}$ ($a_{1,1}$) matrix element going to infinity [26, 27].

We determine the K-matrix by decomposing the full wave function $\psi(r,\theta)$ into partial waves,

$$\psi(r,\theta) = \sum_{l'} \frac{u_{l'}(r)}{r} Y_{l',0}(\cos\theta), \tag{10}$$

where the sum over l' includes all angular momentum values allowed by symmetry and where the spherical harmonics Y_{l',m'_l} are independent of ϕ since m'_l is assumed to be zero throughout. Inserting Eq. (10) into the Schrödinger equation $H\psi = E\psi$ and projecting onto the $Y^*_{l,0}$ states, we obtain a set of coupled differential equations for the radial components $u_l(r)$,

$$\left(-\frac{\hbar^2}{2\mu}\frac{\partial^2}{\partial r^2} + V_{2\mathrm{b}}(r)\right) u_l(r) - \frac{1}{2}|\epsilon_{0,\mathrm{S}}|^2 \sum_{l'} W_{l,l'}(r) u_{l'}(r) = E u_l(r). \tag{11}$$

An explicit expression for the coupling matrix elements $W_{l,l'}(r)$, which arise from integrating over the angular degrees of freedom, is given in Appendix A. Equation (A5) shows that the laser-molecule interaction V_{lm} couples only channels with the same l or channels whose indices differ by two. Imposing that the $u_l(r)$ vanish at small r, the logarithmic derivative matrix is propagated using the Johnson algorithm [28] with adjustable step size. Matching the large-r solution to the asymptotic free-particle solution, the K-matrix is extracted. We find that a scattering energy of $10^{-12} a.u.$ approximates the zero-energy limit accurately; for this energy, we choose the large-r matching point to be $10^6 a.u.$. We find that the inclusion of about 8 even and/or 8 odd partial wave channels yields converged results for the field strengths considered in this work.

C. Bound States

In addition to the scattering states, we calculate the bound states of the helium-helium systems in a static external field. Since a time-dependent external field can, at each time, be thought of as being static, the solutions for the static Hamiltonian provide guidance for interpreting our time-dependent results. In the extreme case of an adiabatically changing external field, the full dynamics can be readily extracted from the static results by, e.g., performing a Landau-Zener analysis.

To determine the bound state spectrum, we express the eigen states $\psi(r,\theta)$ in terms of a B-spline basis using non-linear grids in r and θ. The largest r is adjusted so that the most weakly-bound state is fully covered by the numerical grid. For ^{4}He-^{4}He, we calculate eigen states that are even in the relative coordinate z. For the ^{3}He-^{3}He and ^{3}He-^{4}He systems, both even and odd states in z are considered. In the case of ^{3}He-^{3}He, the even and odd partial waves must be combined with singlet and triplet nuclear spin states, respectively. Even though the bound states cannot be labeled by a single l quantum number due to the θ-dependence of V_{lm}, the weakly-bound states are typically dominated by a single partial wave. The dominant character can be obtained by projecting the eigen states onto different l channels.

D. Dynamics

If the laser-molecule interaction is time dependent, we have to solve the time-dependent Schrödinger equation for a given initial state $\Psi(r,\theta,t=-\infty)$. In practice, the initial state is prepared at a time where the laser-molecule interaction can be neglected, i.e., at a time much smaller than 0.

To solve the time-dependent Schrödinger equation, we decompose the wave packet $\Psi(r,\theta,t)$, similar to what we did in Sec. II B to obtain the time-independent scattering states, into partial wave components,

$$\Psi(r,\theta,t) = \sum_{l'} \frac{U_{l'}(r,t)}{r} Y_{l',0}(\cos\theta). \tag{12}$$

Inserting Eq. (12) into the time-dependent Schrödinger equation $\imath\hbar\partial\Psi/\partial t = H\Psi$, we obtain a set of coupled time-dependent equations for the radial components $U_l(r,t)$,

$$\left(-\frac{\hbar^2}{2\mu}\frac{\partial^2}{\partial r^2} + V_{2\mathrm{b}}(r)\right) U_l(r,t) - \frac{1}{2}|\epsilon(t)|^2 \sum_{l'} W_{l,l'}(r) U_{l'}(r,t) = \imath\hbar\frac{\partial U_l(r,t)}{\partial t}, \tag{13}$$

where the coupling elements $W_{l,l'}(r)$ are given in Eq. (A5).

To solve the coupled set of time-dependent radial equations, we discretize the r coordinate (we typically use about 32,000 points) and propagate the $U_l(r,t)$ by expanding the radial propagator in terms of Chebychev polynomials [29]. The time step Δt is chosen such that $|\epsilon(t)|^2$ can be considered, to a very good approximation, as time independent during each time step. We use $\Delta t \approx 0.24$ fs to 0.60 fs and about 30 terms in the expansion into Chebychev polynomials. For the pulses considered, accounting for about eight partial wave channels yields converged results.

III. TIME-INDEPENDENT FIELD STRENGTH

This section discusses the characteristics of the helium-helium systems in the presence of a static external field (parametrization 1. in Sec. II A). Figure 2 shows the dimer binding energy E_{bind} for (a) ^{4}He-^{4}He, (b) ^{3}He-^{4}He, and (c) ^{3}He-^{3}He as a function of the field strength $\epsilon_{0,\mathrm{S}}$. The binding energy associated with states that

are even in z is shown by solid lines and that associated with states that are odd in z is shown by dashed lines. The ^{4}He-^{4}He system supports new s-wave ($l = 0$) dominated bound states for field strengths larger than about $\epsilon_{0,S} = 0.0715 a.u.$ and larger than about $\epsilon_{0,S} = 0.0976 a.u.$. No evidence for the existence of these states is reported in Ref. [13]. For field strengths larger than about $\epsilon_{0,S} = 0.10962 a.u.$, a new bound state with appreciable d-wave admixture is being supported [also notice the related avoided crossing between the s-wave dominated and d-wave dominated states at $(\epsilon_{0,S}, E_{\rm bind}) \approx (0.11 a.u., 5 \times 10^{-7} a.u.)$]. Owing to the orbital angular momentum barrier, this bound state acquires an appreciable binding energy over a fairly small variation of the field strength $\epsilon_{0,S}$. Reference [13] refers to this d-wave dominated state as a "pendular state".

The ^{3}He-^{4}He system [see Fig. 2(b)] supports its first s-wave dominated bound state for field strengths larger than about $\epsilon_{0,S} = 0.0311 a.u.$, a second s-wave dominated bound state for field strengths larger than about $\epsilon_{0,S} = 0.0776 a.u.$, and a third s-wave dominated bound state for field strengths larger than about $\epsilon_{0,S} = 0.1054 a.u.$. Owing to the smaller reduced mass, the latter two field strenths are a bit larger than the critical field strengths for the ^{4}He-^{4}He system. The first field-induced bound state, which first appears at $\epsilon_{0,S} = 0.0311 a.u.$, has no analog in the ^{4}He-^{4}He system since this system already supports a weakly bound state in the absence of an external electric field. The ^{3}He-^{4}He system additionally supports bound states that are odd in the relative coordinate z [see the dashed lines in Fig. 2(b)]. Interestingly, these odd-z bound states first appear at field strengths that are just a bit larger than the field strengths at which the even-z bound states first appear. As the binding energy increases, the energy difference, normalized by the binding energy itself, between the pairs of even-z and odd-z states decreases. This is not unlike the tunneling splitting in a double-well potential, where the tunneling is much smaller for deep-lying states than for states that lie near or above the barrier.

Last, the ^{3}He-^{3}He system first supports even-z bound states at field strengths larger than about $\epsilon_{0,S} = 0.0388 a.u.$, larger than about $0.0832 a.u.$, and larger than about $0.1126 a.u.$, respectively. Odd-z bound states are first supported at field strengths larger than about $\epsilon_{0,S} = 0.0492294 a.u.$, larger than about $\epsilon_{0,S} = 0.0875679 a.u.$, and larger than about $\epsilon_{0,S} = 0.116342 a.u.$. Owing to the smaller reduced mass, these field strenths are a bit larger than the corresponding critical field strengths for the ^{3}He-^{4}He system.

As mentioned in Sec. II B, the emergence of a new even-z bound state is accompanied by a diverging $a_{0,0}$ and the emergence of a new odd-z bound state by a diverging $a_{1,1}$. Solid lines in Fig. 3 show the scattering length matrix element $a_{0,0}$ as a function of the field strength $\epsilon_{0,S}$ for (a) ^{4}He-^{4}He, (b) ^{3}He-^{4}He, and (d) ^{3}He-^{3}He while dashed lines show the scattering length matrix element $a_{1,1}$ for (c) ^{3}He-^{4}He and (e) ^{3}He-^{3}He. Comparison with Fig. 2

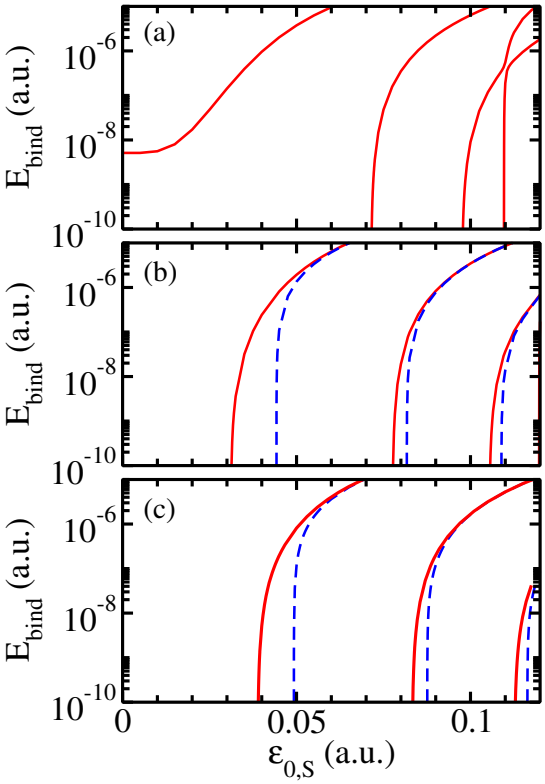

FIG. 2: (color online) Binding energy $E_{\rm bind}$ for (a) ^{4}He-^{4}He, (b) ^{3}He-^{4}He, and (c) ^{3}He-^{3}He as a function of the field strength $\epsilon_{0,S}$. The solid lines show the binding energy of states that are even in z while the dashed lines show the binding energy of states that are odd in z. Note that the binding energy is shown on a logarithmic scale that covers five orders of magnitude.

shows that $a_{0,0}$ and $a_{1,1}$ go through infinity at the field strengths at which new, respectively, even-z and odd-z bound states are first being supported. We checked that the generalized scattering lengths $a_{l,l'}$, except for $a_{0,0}$, are well described—as they should be for potentials that are purely dipolar at large internuclear distances [23]—by the Born approximation for field strengths where resonances are absent. This is illustrated in Figs. 3(c) and 3(e), where the Born approximation results (solid circles) reproduce the full coupled-channel calculations (dashed lines) reliably. In the Born approximation, $a_{1,1}$ is given by $-2\mu|\epsilon_{0,S}|^2|\alpha_0|^2/[5(4\pi\mathcal{E}_0)^2\hbar^2]$ [30]. Figure 4 shows an enlargement of the scattering length matrix element $a_{1,1}$ for ^{3}He-^{4}He near the third resonance shown in Fig. 3(c), i.e., near $\epsilon_{0,S} \approx 0.10885 a.u.$. The Born approximation values do not capture the resonance; instead, they continue to change quadratically with $\epsilon_{0,S}$ across the reso-

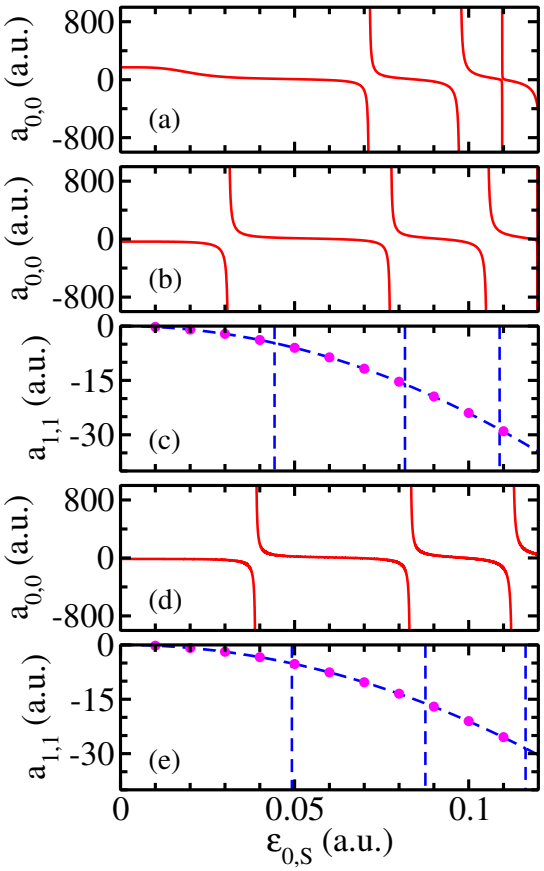

FIG. 3: (Color online) Scattering lengths for (a) ^{4}He-^{4}He, (b) and (c) ^{3}He-^{4}He, and (d) and (e) ^{3}He-^{3}He as a function of the field strength $\epsilon_{0,S}$. The solid lines in (a), (b), and (d) show the scattering length $a_{0,0}$ while the dashed lines in (c) and (e) show the scattering length $a_{1,1}$. The narrow resonance at $\epsilon_{0,S} \approx 0.11 a.u.$ in (a) has notable d-wave admixture. The resonances in the $(l, l') = (1, 1)$ channel [see panels (c) and (e)] are extremely narrow. The solid circles in panels (c) and (e) show $a_{1,1}$ as predicted by the Born approximation; the Born approximation reproduces the "background value" very well but does not capture the resonances (the scattering lengths in the Born approximation are directly proportional to $-|\epsilon_{0,S}|^2$).

nance.

The calculations presented thus far employ the *ab initio* polarization model from Ref. [20]. If we use the simpler analytical polarization model [Eqs. (2) and (3)], the first electric-field induced resonance for ^{4}He-^{4}He occurs at $\epsilon_{0,S} = 0.0699 a.u.$ instead of at $\epsilon_{0,S} = 0.0715 a.u.$ and the first electric-field induced resonance for ^{3}He-^{4}He occurs at $\epsilon_{0,S} = 0.0304 a.u.$ instead of at $\epsilon_{0,S} = 0.0311 a.u.$. The deviation between the results for the two different polarization models increases with increasing field strength.

Our results for the scattering properties of the ^{3}He-^{4}He and ^{3}He-^{3}He systems in the presence of a static

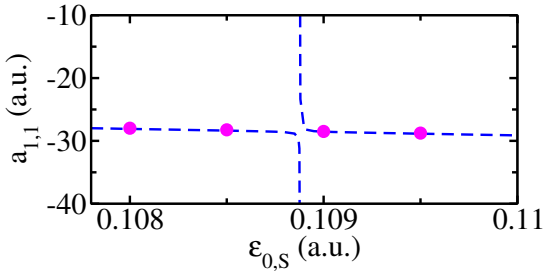

FIG. 4: (Color online) Enlargement of the scattering length $a_{1,1}$ for ^{3}He-^{4}He in the vicinity of a resonance. The data and symbol/line styles are the same as in Fig. 3(c).

field disagree quantitatively with those presented in Ref. [9, 31]. Repeating the calculations for the interactions employed in Ref. [9] (i.e., using the LM2M2 potential [33] and the analytic polarizability model), we find that the first bound state for ^{3}He-^{4}He is supported for $\epsilon_{0,S} = 0.0305 a.u.$ as opposed to $0.053 a.u.$ as reported in Ref. [9] and the first s-wave dominated bound state for ^{3}He-^{3}He first appears at $\epsilon_{0,S} = 0.0382 a.u.$ as opposed to $\epsilon_{0,S} = 0.067 a.u.$ as reported in Ref. [9]. We have no insight into what might be the reason for the discrepancies.

The results presented so far indicate that the helium-helium interaction strength can be varied through the application of a static external field. While the field strengths required are attainable with present-day technology, they can only be realized for a relatively short time. For the field to be considered truly static, the pulse duration has to be longer than the internal or characteristic time scale of the helium-helium system. If we convert the ^{4}He-^{4}He binding energy in the absence of an external field, we find a time scale of about 29.71 ns. Clearly, the realization of such temporally extended, high-intensity laser pulses is presently out of reach. Alternatively, the minimal energy of the He-He interaction potential corresponds to a time scale of about 4.364 ps. This time scale estimate looks much more promising from an experimental point of view. Alternatively, we can estimate the time scale associated with the field-induced bound states. Energies of $10^{-10} a.u.$, $10^{-8} a.u.$, and $10^{-6} a.u.$ correspond to time scales of about $1,520$ ns, 15.20 ns, and 0.1520 ns. If one were to populate the new bound state and if the system could be held at a particular field strength longer than the time given above, one should be able to see revival signatures corresponding to the above time scale in the dynamical evolution of an appropriately chosen observable. While challenging, realizing such a scenario experimentally does not seem entirely out of reach. Ultimately, one has to analyze the full dynamics to see which pulse shapes and lengths yield observable signatures of the electric-field induced tunability of the helium-helium interaction strength. Exploratory calculations along these lines are presented in the next section. While earlier work [32] employed a perturbative framework to address this question, we employ

a full coupled-channel treatment. Our calculations employ peak electric field strengths of $\epsilon_{0,\mathrm{G}} = 0.0843949 a.u.$ and $0.11 a.u.$ (corresponding to $2.5 \times 10^{14}\mathrm{W/cm^2}$ and $4.247 \times 10^{14}\mathrm{W/cm^2}$, respectively). These field strengths are significiantly lower than those employed in "realm II" of Ref. [13].

IV. TIME-DEPENDENT FIELD STRENGTH

This section summarizes our results for the stretched Gaussian pulse (parameterization 2. in Sec. II A). Our studies are motivated by two questions: What, if any, are the signatures of the field-induced resonances discussed in Sec. III that could be measured experimentally in pump-probe experiments? Do the field-induced resonances lead to revival dynamics, somewhat reminiscent of what has been observed in pump-probe experiments for stiff, rigid rotor-like diatomic molecules [34, 35]? To address these questions, we focus on the ^{4}He-^{4}He system. We assume that the dimer is prepared in the absence of an external field in its $l = 0$ ground state, as is being done in molecular beam experiments [1, 5–7, 14]. The laser pulse is then turned on and the system is assumed to be imaged via COLTRIMS after a delay time [14, 36]. In this technique, an extremely short and intense probe pulse, which "rips off" one electron of each of the helium atoms, is applied and the ions are imaged. Since the probe pulse, to a very good approximation, instantaneously projects the helium atoms to one particular configuration, we do not simulate the imaging part of the experiment. Repeated experimental measurements for the same time delay provide access to the quantum mechanical density distribution of the wave packet. In what follows, the delay time is defined such that it is zero when the stretched Gaussian pulse first reaches its maximum. Our calculations scan the delay time from zero to many times t_{hold}.

We monitor the correlator or alignment $C_2(r,t)$,

$$C_2(r,t) = \frac{\int_0^\pi \Psi^*(r,\theta,t)\cos^2\theta\Psi(r,\theta,t)\sin\theta d\theta}{\int_0^\pi |\Psi(r,\theta,t)|^2\sin\theta d\theta}. \quad (14)$$

If Ψ was independent of θ (as it is in the absence of the laser pulse), $C_2(r,t)$ would be equal to 1/3. Deviations from 1/3 provide a measure of the angle dependence that is introduced to the wave packet by the laser pulse. Importantly, after the laser is "off", i.e., after its intensity has decayed to a sufficiently small value, the coupling between different l channels vanishes and the populations of the different l channels are independent of time. The wave packet itself, however, continues to change with time since the spatially-dependent phases of the different partial wave components continue to evolve. These phase factors imprint an r-dependent interference pattern, which varies with time (see also Ref. [14]), onto the correlator $C_2(r,t)$.

The upper row of Fig. 5 shows contour plots of $C_2(r,t)$ for fixed τ and $\epsilon_{0,\mathrm{G}}$, $\tau = 311$fs and $\epsilon_{0,\mathrm{G}} \approx 0.0844 a.u.$ (intensity of $2.5 \times 10^{14}\mathrm{W/cm^2}$), and four different hold times, i.e., for $t_{\mathrm{hold}} = 0.5$ps, 2ps, 4ps, and 8ps. The lines in the lower row show cuts, from bottom to top, for $r = 3\mathring{A} = 5.669 a.u.$, $r = 5\mathring{A} = 9.449 a.u.$, $r = 10\mathring{A} = 18.90 a.u.$, and $r = 20\mathring{A} = 37.79 a.u.$. For the peak field strength used, the static system supports two bound states that are dominated by the s-wave channel (see Figs. 2 and 3).

For the shortest t_{hold} considered, $C_2(r,t)$ is characterized by a fairly regular interference pattern, whose maxima and minima move out with increasing time. Even though t_{hold} is finite, the interference pattern is quite similar to that observed and interpreted in a very recent joint experiment-theory collaboration, which employed an unstretched Gaussian pulse with $t_{\mathrm{hold}} = 0$, the same τ, and comparable field strength [14]. The pattern of the alignment signal can be traced back to the interference between the dissociating $l = 2$ wave packet portion, which gets populated as a consequence of the laser-molecule interaction, and the broad spherically-symmetric background portion (recall, the initial state is a pure s-wave state). Close inspection of $C_2(r,t)$ in the $t = 0.5$ ps to 1 ps window, however, reveals that the interference pattern is due to two dissociating wave packet portions, one that is emitted starting at $t = 0$ and another that is emitted for $t \gtrsim t_{\mathrm{hold}}$. This behavior becomes more prominent for larger t_{hold} (see below).

The small r behavior changes distinctly when t_{hold} increases. Figures 5(b)-5(d) display oscillations of $C_2(r,t)$ at small r [see also the dashed lines in Figs. 5(f)-5(h)]. These oscillations, which are most prominent for the largest hold time considered [Fig. 5(h)], are roughly governed by the binding energy of the deepest-lying, s-wave dominated transient state that is supported by the static Hamiltonian with field strength $\epsilon_{0,\mathrm{G}}$. Its binding energy translates to about 3.800 ps. The time scale associated with the energy difference between the two s-wave dominated transient bound states is equal to about 3.891 ps, which is very close to the time scale set by the binding energy of the deep-lying transient state. Indeed, we attribute the small-r oscillations of $C_2(r,t)$ to two processes, namely the interference between the wave packet portions corresponding to the two transient bound states and the interference between the wave packet portions corresponding to the deep-lying transient bound state and unbound scattering states. These interference processes both contribute to the population transfer between the $l = 0$ and $l = 2$ channels and thus lead to oscillations in the alignment $C_2(r,t)$.

The oscillations of $C_2(r,t)$ are reminiscent of revival dynamics in rigid-rotor like molecules due to population transfer between different rotational states. There are, however, important differences. First, unlike for rigid-rotor molecules where multiple eigen energies with spacings set by the rotational constant B exist in the absence of the field, the deep-lying state that sets the time scale in the helium dimer system is transient. Second, the r-dependence of the alignment $C_2(r,t)$, as highlighted by

the "outgoing finger structure" in Fig. 5, is unique to the non-rigid helium dimer. For rigid-rotor molecules, this structure is absent. Third, the broadness of the initial wave packet combined with the fact that the laser-molecule interaction is dominant at small r implies that only a small fraction of the wave packet gets "promoted" to finite l states.

As already alluded to above, Figs. 5(b)-5(d) show that the decay of the pump pulse from strength $\epsilon_{0,\mathrm{G}}$ to zero (this occurs for times just a bit larger than t_{hold}) triggers the "emission" of a second dissociating wave packet portion, which can be attributed to the fact that the population of the deep-lying transient bound state is no longer bound when the laser intensity is negligible. The second dissociating wave packet produces a new set of outgoing fingers that are delayed by t_{hold} compared to the first set of fingers and that "collide" with the first set of fingers. The interference of the delayed outgoing wave packet portion with the first dissociating wave packet portion leads, as can be seen nicely in the $r = 20\mathring{A}$ cuts [solid lines in Figs. 5(f)-5(h)], to "distorsions" of the interference pattern. In particular, it can be seen that $C_2(r,t)$ displays a regularly changing wave pattern for $t \leq t_{\mathrm{hold}}$ that changes notably for t just a bit larger than t_{hold}. For t quite a bit larger than t_{hold}, $C_2(r,t)$ again displays a regularly changing wave pattern.

Figure 6 shows the same quantities as Fig. 5 but for a larger peak field strength, namely for $\epsilon_{0,\mathrm{G}} = 0.11 a.u.$. For this field strength, the static ^{4}He-^{4}He system supports three s-wave dominated bound states and one d-wave dominated bound state. The binding energy of the most strongly-bound transient state translates to a time scale of 1.522 ps. Indeed, the small-r region of the alignment signal displays close to regular oscillations at roughly this time scale. We do not expect perfect "single-frequency" oscillations since several transient eigen frequencies are expected to contribute to the observed oscillatory pattern. As in the weaker field strength case, the emission of a second dissociating wave packet portion at times just a bit larger than t_{hold} is clearly visible in the alignment signal. Comparison of Figs. 5 and 6 shows that the larger field strength has two primary effects. First, it leads to a shortening of the oscillation period of the small-r portion of $C_2(r,t)$. Second, it enhances the contrast of $C_2(r,t)$. Besides these two effects, the overall behavior of $C_2(r,t)$ is quite similar.

Figures 5 and 6 demonstrate that pump-probe experiments on the ^{4}He-^{4}He system should provide evidence for the tunability of the bound state spectrum by an external electric field. However, the alignment signal does unfortunately not—or if so rather indirectly—provide access to the number of field-induced bound states since the energy level spacing of the field-induced bound states is highly non-linear, leading to vastly different time scales governing the interference between the more weakly bound states. Moreover, the highly non-linear spacing also makes it difficult to distinguish between oscillations in the alignment $C_2(r,t)$ due to the interference of wave packet portions corresponding to the deepest-lying transient state and the most weakly-bound transient state and oscillations in the alignment $C_2(r,t)$ due to the interference of wave packet portions corresponding to the deepest-lying transient state and the transient scattering continuum. The latter process contributes also for peak field strengths $\epsilon_{0,\mathrm{G}}$ that are smaller than $0.0715 a.u.$, i.e., for peak strengths for which the static field Hamiltonian supports only one bound state. However, in this field strength regime, the large time scale associated with the small binding energy makes the unambiguous experimental observation that the energy of the transient bound state has been tuned essentially impossible.

V. CONCLUSION

This work investigated static and dynamic properties of helium-helium systems in the presence of an external electric field. All three possible combinations of the two isotopes ^{3}He and ^{4}He were investigated, namely the ^{4}He-^{4}He, ^{3}He-^{4}He, and ^{3}He-^{3}He systems. In the absence of an external field, only the ^{4}He-^{4}He system supports a weakly-bound state (and only one). When a static external electric field is applied, all three helium-helium systems display field-induced scattering resonances, which are accompanied by the pulling-in of new two-body bound states. The resonances and their characteristics were analyzed carefully.

Applying a stretched Gaussian laser pulse, the work investigated the signatures imprinted on the dynamics by the field-induced resonances. For this analysis, we focused on the ^{4}He-^{4}He system. Assuming that the system is prepared in its only bound state in the absence of an external field, the time evolution during and after the stretched Gaussian pump pulse was investigated. It was found that the time-evolving wave packet carries fingerprints of the field-induced bound states, in addition to displaying dissociative dynamics that is associated with the fact that the pump laser leads to the population of scattering states with zero and finite angular momenta. It was commented that the experimental realization of the simulated scenarios is technically demanding but not impossible.

The response of diatomic rigid rotor-like molecules to intense laser pulses has been studied extensively in the literature, both experimentally and theoretically. The present dynamical study differs from these earlier works in that the ^{4}He-^{4}He system supports only a single extremely weakly-bound state in the absence of an external field. Thus, the notion of a rotor-like spectrum does not apply. As a consequence, the external field leads to a strong coupling of the vibrational and rotational degrees of freedom, with the populations of finite l states dissociating.

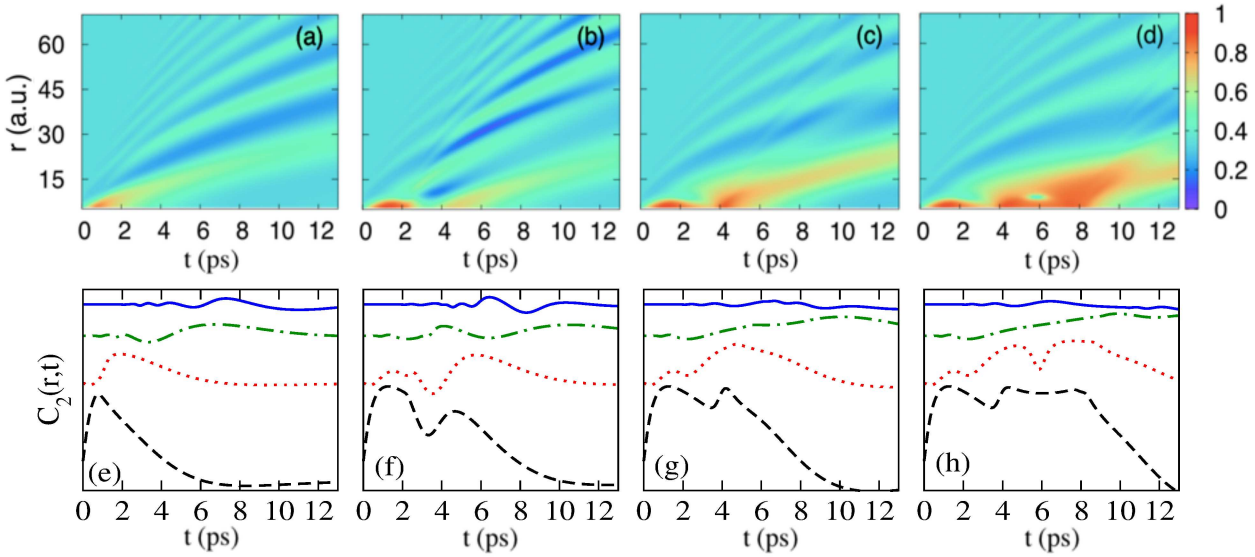

FIG. 5: (Color online) Alignment signal for stretched Gaussian laser pulse with $\epsilon_{0,\mathrm{G}} = 0.0843949 a.u.$ and $\tau = 311$ fs. Results are shown for four different hold times: (a) and (e) $t_{\mathrm{hold}} = 0.5$ ps, (b) and (f) $t_{\mathrm{hold}} = 2$ ps, (c) and (g) $t_{\mathrm{hold}} = 4$ ps, and (d) and (h) $t_{\mathrm{hold}} = 8$ ps. Panels (a)-(d) show contour plots of the alignment signal $C_2(r,t)$. A spherically symmetric wave packet would yield an alignment signal of 1/3. The dashed, dotted, dash-dotted, and solid lines in panels (e)-(h) show cuts of $C_2(r,t)$ for $r = 3\mathring{A} = 5.669 a.u.$, $r = 5\mathring{A} = 9.449 a.u.$, $r = 10\mathring{A} = 18.90 a.u.$, and $r = 20\mathring{A} = 37.79 a.u.$, respectively. The curves are offset from each other for ease of readibility.

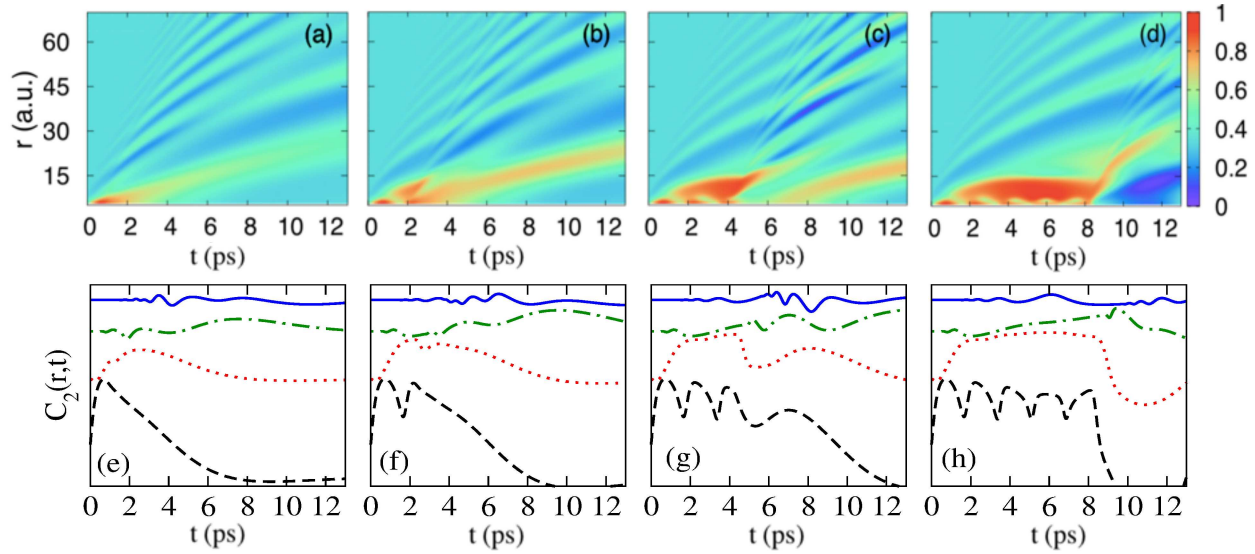

FIG. 6: (Color online) Same as Fig. 5 but for a larger peak field strength, namely for $\epsilon_{0,\mathrm{G}} = 0.11 a.u.$.

VI. ACKNOWLEDGEMENT

We are very grateful to R. Dörner and M. Kunitski for extensive discussions, which motivated and inspired this work. We are also very grateful to D. Fedorov for communication related to Ref. [9]. Support by the National Science Foundation through grant number PHY-1806259 is gratefully acknowledged. This work used the OU Supercomputing Center for Education and Research (OSCER) at the University of Oklahoma (OU).

Appendix A: Coupling Matrix Elements $W_{l,l'}$

To determine explicit expressions for the coupling matrix elements $W_{l,l'}(r)$, we rewrite the laser-molecule interaction $V_{\mathrm{lm}}(r,\theta,t)$ as

$$V_{\mathrm{lm}}(r,\theta,t) = g(t)\left[\alpha_{0,0}(r)Y_{0,0} + \alpha_{2,0}(r)Y_{2,0}(\cos\theta)\right], \quad \text{(A1)}$$

where

$$g(t) = -\frac{|\epsilon(t)|^2}{2}, \quad \text{(A2)}$$

$$\alpha_{0,0}(r) = \frac{\sqrt{4\pi}}{3}\left[\alpha_{\parallel}(r) + 2\alpha_{\perp}(r)\right], \tag{A3}$$

and

$$\alpha_{2,0}(r) = \frac{\sqrt{16\pi}}{3\sqrt{5}}\left[\alpha_{\parallel}(r) - \alpha_{\perp}(r)\right]. \tag{A4}$$

Using this notation, $W_{l,l'}(r)$ becomes

$$W_{l,l'}(r) = \alpha_{0,0}(r)\langle Y_{l,0}|Y_{0,0}|Y_{l',0}\rangle + \alpha_{2,0}(r)\langle Y_{l,0}|Y_{2,0}|Y_{l',0}\rangle, \tag{A5}$$

where the notation $\langle\cdot\rangle$ indicates an integration over the angular degrees of freedom.

[1] W. Schöllkopf and J. P. Toennies, Nondestructive Mass Selection of Small van der Waals Clusters, Science **266**, 1345 (1994).

[2] K. T. Tang, J. P. Toennies, and C. L. Yiu, Accurate Analytical He-He van der Waals Potential Based on Perturbation Theory, Phys. Rev. Lett. **74**, 1546 (1995).

[3] A. R. Janzen and R. A. Aziz, Modern He-He potentials: Another look at binding energy, effective range theory, retardation, and Efimov states, J. Chem. Phys. **103**, 9626 (1995).

[4] F. Luo, C. F. Giese, and W. R. Gentry, Direct measurement of the size of the helium dimer, J. Chem. Phys. **104**, 1151 (1996).

[5] W. Schöllkopf and J. P. Toennies, The nondestructive detection of the helium dimer and trimer, J. Chem. Phys. **104**, 1155 (1996).

[6] R. E. Grisenti, W. Schöllkopf, J. P. Toennies, G. C. Hegerfeldt, T. Köhler, and M. Stoll, Determination of the bond length and binding energy of the helium dimer by diffraction from a transmission grating, Phys. Rev. Lett. **85**, 2284 (2000).

[7] S. Zeller, M. Kunitski, J. Voigtsberger, A. Kalinin, A. Schottelius, C. Schober, M. Waitz, H. Sann, A. Hartung, T. Bauer, M. Pitzer, F. Trinter, C. Goihl, C. Janke, M. Richter, G. Kastirke, M. Weller, A. Czasch, M. Kitzler, M. Braune, R. E. Grisenti, W. Schöllkopf, L. Ph. H. Schmidt, M. S. Schöffler, J. B. Williams, T. Jahnke, and R. Dörner, Imaging the He_2 quantum halo state using a free electron laser, PNAS **113**, 14651 (2016).

[8] C. Chin, R. Grimm, P. Julienne, and E. Tiesinga, Feshbach resonances in ultracold gases, Rev. Mod. Phys. **82**, 1225 (2010).

[9] E. Nielsen, D. V. Fedorov, and A. S. Jensen, Efimov States in External Fields, Phys. Rev. Lett. **82**, 2844 (1999).

[10] V. Efimov, Energy levels arising from resonant two-body forces in a three-body system, Phys. Lett. B **33**, 563 (1970).

[11] E. Braaten and H.-W. Hammer, Universality in few-body systems with large scattering length, Phys. Rep. **428**, 259 (2006).

[12] P. Naidon and S. Endo, Efimov Physics: a review, Rep. Prog. Phys. **80**, 056001 (2017).

[13] Q. Wei, S. Kais, T. Yasuike, and D. Herschbach, Pendular alignment and strong chemical binding are induced in helium dimer molecules by intense laser fields, PNAS **115**, E9058 (2018).

[14] M. Kunitski, Q. Guan, H. Maschkiwitz, J. Hahnenbruch, S. Echart, S. Zeller, A. Kalinin, M. Schöffler, L. Ph. H. Schmidt, T. Jahnke, D. Blume, and R. Dörner, unpublished (2018).

[15] B. Friedrich, M. Gupta, and D. Herschbach, Probing Weakly-Bound Species with Nonresonant Light: Dissociation of He_2 Induced by Rotational Hybridization, Collect. Czech. Chem. Commun. **63**, 1089 (1998).

[16] A. Spott, A. Jaron-Becker, and A. Becker, Time-dependent susceptibility of a helium atom in intense laser pulses, Phys. Rev. A **96**, 053404 (2017).

[17] W. Cencek, M. Przybytek, J. Komasa, J. B. Mehl, B. Jeziorski, and K. Szalewicz, Effects of adiabatic, relativistic, and quantum electrodynamics interactions on the pair potential and thermophysical properties of helium, J. Chem. Phys. **136**, 224303 (2012).

[18] B. Friedrich and D. Herschbach, Alignment and Trapping of Molecules in Intense Laser Fields, Phys. Rev. Lett. **74**, 4623 (1995).

[19] A. D. Buckingham and R. S. Watts, The polarizability of a pair of helium atoms, Mol. Phys. **26**, 7 (1973).

[20] W. Cencek, J. Komasa, and K. Szalewicz, Collision-induced dipole polarizability of helium dimer from explicitly correlated calculations J. Chem. Phys. **135**, 014301 (2011).

[21] J. Weiner, V. S. Bagnato, S. Zilio, and P. S. Julienne, Experiments and theory in cold and ultracold collisions, Rev. Mod. Phys. **71**, 1 (1999).

[22] M. Marinescu and L. You, Controlling Atom-Atom Interaction at Ultralow Temperatures by dc Electric Fields, Phys. Rev. Lett. **81**, 4596 (1998).

[23] S. Yi and L. You, Trapped condensates of atoms with dipole interactions, Phys. Rev. A **63**, 053607 (2001).

[24] B. Deb and L. You, Low-energy atomic collision with dipole interactions, Phys. Rev. A **64**, 022717 (2001).

[25] R. G. Newton, Scattering Theory of Waves and Particles, Dover Publications, Inc., Mineola, New York, 2nd Ed. (2002).

[26] C. Ticknor and J. L. Bohn, Long-range scattering resonances in strong-field-seeking states of polar molecules, Phys. Rev. A **72**, 032717 (2005).

[27] K. Kanjilal and D. Blume, Low-energy resonances and bound states of aligned bosonic and fermionic dipoles, Phys. Rev. A **78**, 040703(R) (2008).

[28] B. R. Johnson, The multichannel log-derivative method for scattering calculations, J. Comp. Phys. **13**, 445 (1973).

[29] T. H. Ezer and R. Kosloff, An accurate and effcient scheme for propagating the time dependent Schrödinger equation, J. Chem. Phys. **81**, 3967 (1984).
[30] K. Kanjilal, J. L. Bohn, and D. Blume, Pseudopotential treatment of two aligned dipoles under external harmonic confinement, Phys. Rev. A **75**, 052705 (2007).
[31] Note that the s-wave scattering length defined in Ref. [9] differs by a minus sign from our definition.
[32] L. W. Bruch, Electric field effects on the helium dimer, J. Chem. Phys. **112**, 9773 (2000).
[33] R. A. Aziz and M. J. Slaman, An examination of ab initio results for the helium potential energy curve, J. Chem. Phys. **94**, 8047 (1991).
[34] H. Stapelfeldt and T. Seideman, *Colloquium*: Aligning molecules with strong laser pulses, Rev. Mod. Phys. **75**, 543 (2003).
[35] M. Lemeshko, R. V. Krems, J. M. Doyle, and S. Kais, Manipulation of molecules with electromagnetic fields, Mol. Phys. **111**, 1648 (2013).
[36] J. Ullrich, R. Moshammer, R. Dörner, O. Jagutzki, V. Mergel, H. Schmidt-Böcking, and L. Spielberger, Recoil-ion momentum spectroscopy, J. Phys. B **30**, 2917 (1997).